Korean J. Chem. Eng., 37(9), 1490-1497 (2020)
DOI: 10.1007/s11814-020-0536-z

pISSN: 0256-1115
eISSN: 1975-7220

Coke combustion kinetics of spent Pt-Sn/Al_2O_3 catalysts in propane dehydrogenation

Pajri Samsi Nasution*,‡, Jae-Won Jung*,‡, Kyeongseok Oh, and Hyoung Lim Koh*,†**

*Department of Chemical Engineering, RCCT, Hankyong National University, Anseong 456-749, Korea
**Chemical and Environmental Technology Department, Inha Technical College,
Inha-ro 100, Michuhol-gu, Incheon 22212, Korea
(*Received 16 December 2019 • Revised 20 February 2020 • Accepted 8 March 2020*)

Abstract−The kinetics of coke combustion was investigated by using a thermogravimetric analyzer (TGA) of coked catalysts which was used for propane dehydrogenation to determine the activation energy. Apart from the Pt/Al_2O_3 catalyst, four different Pt-Sn/Al_2O_3 catalysts were prepared by varying the Pt/Sn ratio from 3 : 0.5 to 3 : 3 by weight. The catalytic activity was measured by propane dehydrogenation at 620 °C. The reactant mixture consisting of C_3H_8 (30 ml/min) and H_2 (30 ml/min) was fed into the reactor for 5 h. A thermogravimetric analyzer in the presence of air was used to determine the amount of coke deposited and calculate the kinetic parameters for coke combustion. Three non-isothermal models (Friedman, Flynn-Wall-Ozawa (FWO), and Kissinger-Akahira-Sunose) were used to determine the activation energy and the best model to fit the experimental data. The FWO model provided the best fit for 3Pt/Al_2O_3 and 3Pt-0.5Sn/Al_2O_3. The three models were equivalent for fitting the data for 3Pt-1Sn/Al_2O_3, 3Pt-2Sn/Al_2O_3, and 3Pt-3Sn/Al_2O_3. The activation energy increased with increasing Sn addition in the 3Pt/Al_2O_3 catalyst. Differences in the locations and the qualitative features of the cokes were suggested to interpret the results.

Keywords: Coke Combustion, Propane Dehydrogenation, Pt-Sn/Al_2O_3, Thermogravimetry, Activation Energy

INTRODUCTION

Light olefins like ethylene and propylene are very important chemical intermediates with a demand that continues to increase. Since 2010, the advantage of dehydrogenation processes of propane in shale gas has gained increasing attention, as this gas contains significant amounts of propane and butane, even though the main product of shale gas is methane [1-3]. With the lower price of propane, the propylene supply is also becoming important. Propane dehydrogenation (PDH) to produce propylene has attracted much attention. In commercial plants, the PDH process is performed with Pt or Cr catalysts, but the demand for highly active catalysts is still growing [4-6]. Nevertheless, coke generation during the PDH process appears to be inevitable because dehydrogenation is very endothermic and requires high temperatures. Bimetallic catalysts such as Pt-Sn catalysts have been examined to delay coke deposit. The advantages of bimetallic catalysts include enhancement of the propane conversion and propylene selectivity [5,7].

Wang et al. [8] analyzed the coke forms generated during the PDH process and classified three types of cokes qualitatively. Even though analysis of the location of coke generated during the PDH reaction is complicated, they also tried to identify the locations in the catalysts. They reported that coke was generated on the metal, in the vicinity of the metal, and also on the support. The chemical components of the cokes were also classified as aliphatic, aromatic, and pre-graphite. At prolonged reaction times, aliphatic coke may be converted to either aromatic or pre-graphite. Though unconfirmed, the metal dispersion might affect the coke generation. In our previous study [7], the metal dispersion was changed by varying the treatment temperature from 450 to 600 °C in the range of direct reduction. From a qualitative study of the coke location, we reported that the so-called drain effect may provide indirect evidence that differences in the coke combustion observed by differential thermal analysis (DTA) are caused by the coke location. A split of the DTA peak was observed at 400-500 °C and was unique in case of bimetallic Pt-Sn catalysts. With addition of Sn, peak splits were clearly observed in the DTA analysis. The observed peak splits were attributed to the migration of coke. However, there was no evidence that the type of coke differed with the addition of a Sn promoter. More coke was also noticed on the metal catalyst when it was suspected that the Pt_3Sn alloy was present and coke accumulation was more active.

Kinetic studies on the combustion of coke are important in the design of PDH regenerator in which PDH catalyst can be regenerated by burning the coke on the catalyst. Since the PDH process could be improved into a continuous process by the regenerator, a regenerator is essential for efficient PDH process. Kinetic studies on the coke combustion in the study of catalysts have been carried out mainly so far for the fluid catalytic cracking [9-13] or paraffin dehydrogenation or naphtha reforming catalyst [14,15]. Ochor et al. [9] conducted a study of the kinetic parameters for fluid catalytic cracking reactions using three methods, i.e., the kinetic model-based, iso-conversional, and modulated methods, using TGA data and analyzed their advantages and disadvantages. Luo et al. [16] conducted a kinetic study on the oxidation of coke produced by the long-chain dehydrogenation of PtSn catalysts. The coke types were classified as coke on metal, on carrier, and away from platinum,

†To whom correspondence should be addressed.
E-mail: hlkoh@hknu.ac.kr
‡Both authors contributed equally as the first author.

and the reaction orders were obtained for each coke type and oxygen. Zagoruiko et al. [14] also conducted a kinetics study of the oxidation of coke produced in the naphtha reforming reaction and designed a regeneration process using the obtained kinematic variables. However, there have been no kinetics studies on the oxidation of coke produced by propane dehydrogenation on PtSn/alumina catalysts. In the kinetics study of a single reaction or single component, there is usually single activation energy for conversion or reaction. In contrast, the activation energy of multi-component mixtures varies according to the temperature. For instance, oil products from kerogen retorting [17], polymer pyrolysis [18,19], and biomass pyrolysis [20,21] showed multiple activation energies as a function of the temperature. As non-isothermal models for analyzing the kinetics, the Friedman, Flynn-Wall-Ozawa (FWO), and Kissinger-Akahira-Sunose (KAS) methods are frequently used to determine the activation energies with variation of the temperature [18-21].

In this study, thermal gravimetric analysis was adopted to study the non-isothermal kinetics of coke combustion. Cokes were generated from the PDH process in the presence of Pt and bimetallic Pt-Sn catalysts. The kinetic variables influencing coke formation on catalysts are of interest. Apart from the Pt/Al_2O_3 catalyst, four different $Pt\text{-}Sn/Al_2O_3$ catalysts were prepared by varying the Pt/Sn ratio from 3 : 0.5 to 3 : 3 by weight. The spent catalysts after the PDH reaction were evaluated. Thermal gravimetric analysis was employed to determine the amount of coke deposited and to calculate the kinetic parameters of coke combustion. Three non-isothermal models (Friedman, FWO, and KAS) were used to determine the activation energy and the best model to fit the experimental data.

EXPERIMENTAL

1. Catalyst Preparation

The current investigation involved dehydrogenating propane and combusting the coked $Pt\text{-}Sn/Al_2O_3$ catalysts for kinetics analysis of coke combustion for the used catalyst. The catalyst was prepared by using a previously described method [7]. Predetermined amounts of $H_2PtCl_6{\cdot}6H_2O$ (Sigma-Aldrich, ≥37.5% Pt basis) and $SnCl_2{\cdot}2H_2O$ (Sigma-Aldrich, ≥98%) were dissolved in 1.5 ml of anhydrous ethanol (C_2H_5OH, 99.5%, Daejung). The precursor solution was then evenly dispersed over a 3.00 g θ-Al_2O_3 support placed in a plastic tube. The mixture was homogenized by manually shaking for ca. 5 min. The catalysts were dried in a drying oven for 24 h before drying at 120 °C. The catalysts were calcined by heating from room temperature to 600 °C (at rate of 10 °C min^{-1}), maintained at 600 °C for 4 h, and cooled to room temperature at a rate of 5 °C min^{-1} for 2 h. In laboratory studies, up to 3 wt% of Pt on Al_2O_3 supports is often employed in the PDH reaction, which is higher than the Pt content (less than 1 wt%) of industrial catalysts. Herein, 3 wt% Pt was selected as a reference catalyst and Sn metal was added as a co-catalyst in the range of 0.5-3 wt%. The prepared catalysts are denoted as $3Pt/Al_2O_3$, $3Pt\text{-}0.5Sn/Al_2O_3$, $3Pt\text{-}1Sn/Al_2O_3$, $3Pt\text{-}2Sn/Al_2O_3$, and $3Pt\text{-}3Sn/Al_2O_3$.

2. Catalyst Performance in Propane Dehydrogenation

Propane dehydrogenation was performed in a fixed-bed reactor at 1 bar and 600 °C. The catalyst (100 mg) was placed into a quartz reactor inside a furnace. The temperature was increased to 600 °C at 10 °C min^{-1} while H_2 gas at a flow rate of 30 ml min^{-1} was used to reduce the catalyst. The reaction mixture consisting of C_3H_8 (30 ml min^{-1}) and H_2 (30 ml min^{-1}) was fed into the reactor for 5 h. The product was sampled at different intervals and analyzed by gas chromatography with a flame ionization detector. The propane conversion and propylene selectivity were calculated by using the following formulas:

$$\text{Propane conversion (\%)} = \frac{n(C_3H_8)_{in} - n(C_3H_8)_{out}}{n(C_3H_8)_{in}} \times 100 \quad (1)$$

$$\text{Propylene selectivity (\%)} = \frac{n(C_3H_6)_{out}}{n(C_2H_6)_{out} + n(C_2H_6)_{out} + n(C_2H_4)_{out} + n(CH_4)_{out}} \times 100 \quad (2)$$

where $n(C_3H_8)_{in}$ and $n(C_xH_y)_{out}$ are the moles of propane from the inlet and number of moles of products from the outlet, respectively.

3. Thermogravimetric Analysis (TGA)

The deactivated catalysts were subjected to TGA using a Perkin Elmer TGA 7 instrument. In order to eliminate the effect of internal diffusion on the intrinsic kinetics, the used catalysts were ground and sieved to a size of 75-105 μm. The fine sample with a weight of ~6.0 mg was heated from ambient temperature to 800 °C at heating rates of 5, 10, and 15 °C min^{-1} while purging with air at 50 ml min^{-1}. The TGA data were saved and processed in a spreadsheet software to calculate the reaction kinetics parameters.

4. Kinetics Analysis from TGA

Iso-conversional kinetics are usually analyzed based on the degree of conversion. The TGA data must be converted from weight loss to the degree of conversion (α), where α increases from 0 to 1. The derivative conversion curve can provide information about the conversion rate, which may be more sensitive to the present reaction conditions [18-21].

4-1. Kinetics Modeling of Coke Combustion

The kinetics equation for thermal decomposition of solid-state matter is expressed as the rate of conversion, as shown in Eq. (3):

$$\frac{d\alpha}{dt} = k(T)f(\alpha) \quad (3)$$

where t, α, and T represent the time, the extent of the reaction, and temperature, respectively. On the right-hand side, k(T) is the temperature-dependent rate constant and $f(\alpha)$ is a function that represents the reaction model, as shown in Table 1. The extent of the reaction, α, can be expressed as Eq. (4).

$$\alpha = \frac{m_o - m_t}{m_o - m_f} \quad (4)$$

where, m_o is the initial mass of the sample, m_f is the final mass of the sample at the end of the reaction, and m_t is the mass of the sample at time t. The reaction rate constant is temperature-dependent and can be expressed by the Arrhenius equation as follows:

$$k(T) = A\exp\left(\frac{-E_a}{RT}\right) \quad (5)$$

where, E_a (J mol^{-1}) is the activation energy of the reaction, A is the pre-exponential factor, and R (J mol^{-1} K^{-1}) is the universal gas constant. Eqs. (3) and (5) can be combined to give to Eq. (6).

Table 1. Kinetics models applied to TGA analysis, where f(α) is shown in Eq. (3) and g(α) is the integral form of f(α) [refer to 18-21]

	Reaction model	Code	f(α)	g(α)
1	Power law	P4	$4\alpha^{3/4}$	$\alpha^{1/4}$
2	Power law	P3	$3\alpha^{2/3}$	$\alpha^{1/3}$
3	Power law	P2	$2\alpha^{1/2}$	$\alpha^{1/2}$
4	Power law	P2/3	$2/3\alpha^{-1/4}$	$\alpha^{3/2}$
5	Maple (first order)	F1	$1-\alpha$	$-\ln(1-\alpha)$
6	Avrami-Erofeev	A2	$2(1-\alpha)\,[-\ln(1-\alpha)]^{1/2}$	$[-\ln(1-\alpha)]^{1/2}$
7	Avrami-Erofeev	A3	$3(1-\alpha)\,[-\ln(1-\alpha)]^{2/4}$	$[-\ln(1-\alpha)]^{1/3}$
8	Avrami-Erofeev	A4	$4(1-\alpha)\,[-\ln(1-\alpha)]^{3/4}$	$[-\ln(1-\alpha)]^{1/4}$
9	Contracting cylinder	R2	$2(1-\alpha)^{1/2}$	$1-(1-\alpha)^{1/2}$
10	Contracting sphere	R3	$3(1-\alpha)^{2/3}$	$1-(1-\alpha)^{1/3}$
11	One-dimensional diffusion	D1	$1/2\ \alpha^{-1}$	α^2
12	Two-dimensional diffusion	D2	$[-\ln(1-\alpha)]^{-1}$	$(1-\alpha)\ln(1-\alpha)+\alpha$
13	Three-dimensional diffusion	D3	$3/2(1-\alpha)^{2/3}\,[1-(1-\alpha)^{1/3}]^{-1}$	$[1-(1-\alpha)^{1/3}]^2$

$$\frac{d\alpha}{dt} = A\exp\left(\frac{-E_a}{RT}\right)f(\alpha) \tag{6}$$

If the heating rate, β (K min^{-1}), is constant, β can be defined by Eq. (7).

$$\beta = \frac{dT}{dt} = \frac{dT}{d\alpha}\cdot\frac{d\alpha}{dt} \tag{7}$$

When Eq. (7) is introduced into Eq. (6), Eq. (8) can be obtained as shown below.

$$\frac{d\alpha}{dT} = \frac{A}{\beta}\exp\left(\frac{-E_a}{RT}\right)f(\alpha) \tag{8}$$

Eq. (8) can be solved by two approaches: the so-called different iso-conversional method and integral iso-conversional method. The respective methods are discussed below.

4-2. Differential Iso-conversional Method

Friedman [22] introduced the most common differential iso-conversional method (FR method), which uses the log of Eq. (6) on both sides:

$$\ln\left(\frac{d\alpha}{dt}\right)_{\alpha,i} = \ln[f(\alpha)A_\alpha] - \frac{E_a}{RT_{\alpha,i}} \tag{9}$$

The subscript *i* in Eq. (9) represents any heating rate temperature program that can be applied at the respective α. The value of E_a at each given α is determined from the slope of the linear plot of ln $(d\alpha/dt)_{\alpha,i}$ vs. $1/T_{a,i}$. Here, $T_{a,i}$ is the temperature at which the conversion α is achieved at the heating rate *i*. Because β=dT/dt, the variable $\ln(d\alpha/dt)_{\alpha,i}$ adopts the form of $\ln\beta\,(d\alpha/dT)_{\alpha,i}$.

4-3. Integral Iso-conversional Method

The integral iso-conversional method is derived from the application of the iso-conversional principle to the integral of Eq. (8), which leads to:

$$g(\alpha) = \int_0^\alpha \frac{d\alpha}{f(\alpha)} = \frac{A}{\beta}\int_{T_0}^{T}\exp\left(\frac{-E_a}{RT}\right)dT \tag{10}$$

Integration of the right-hand side Eq. (10) does not have an analytical solution for an arbitrary temperature program. For this reason, there are a number of approximated solutions that differ in terms of the integral method presented in Eq. (8). One popular integral iso-conversional method was proposed by Kissinger [23] and Akahira and Sunose [24], called the KAS method, and is expressed as follows:

$$\ln\frac{\beta}{T_{\alpha,i}^2} = \ln\left(\frac{RA_\alpha}{E_\alpha g(\alpha)}\right) - \left(\frac{E_a}{RT_\alpha}\right) \tag{11}$$

where, the plot ln (β/T^2) vs. 1/T provides the slope that is used to determine the activation energy, E_a. In another approach, the Flynn-Wall-Ozawa (FWO) method [25,26] was derived from Doyle's approximation [27] with Eq. (10); the logarithmic form of the reaction rate is expressed as:

$$\ln\beta_i = \ln\left(\frac{A_\alpha\cdot E_a}{Rg(\alpha)}\right) - 5.331 - 1.052\left(\frac{E_a}{RT}\right) \tag{12}$$

The KAS method and FWO method are simply reduced to Eq. (13) as shown below.

$$\ln\frac{\beta}{T_{\alpha,i}^B} = \text{constant} - C\left(\frac{E_\alpha}{RT}\right) \tag{13}$$

Here, the values of B and C in Eq. (1) are 2 and 1 for the KAS method and 0 and 1.052 for the FWO method, respectively. The apparent activation energy, E_a, at a constant value of α is obtained from the slope of the plot of ln β vs. 1/T using at least three different heating rates. The Kissinger equation is expressed as:

$$\ln\frac{\beta}{T_{m,i}^2} = \ln\left(\frac{AR}{E_\alpha}\right) - \left(\frac{E_\alpha}{RT_{m,i}}\right) \tag{14}$$

Here, T_m is the temperature where $d\alpha/dt$ is maximal. The slope of the plot of the left side of Eq. (14) vs. $1/T_m$ provides the activation energy.

RESULTS AND DISCUSSION

PDH experiments with five catalysts were performed for 5 h; the propane conversion and propylene selectivity data are presented in Fig. 1 and Fig. 2, respectively. The Pt/Al_2O_3 catalyst as a reference

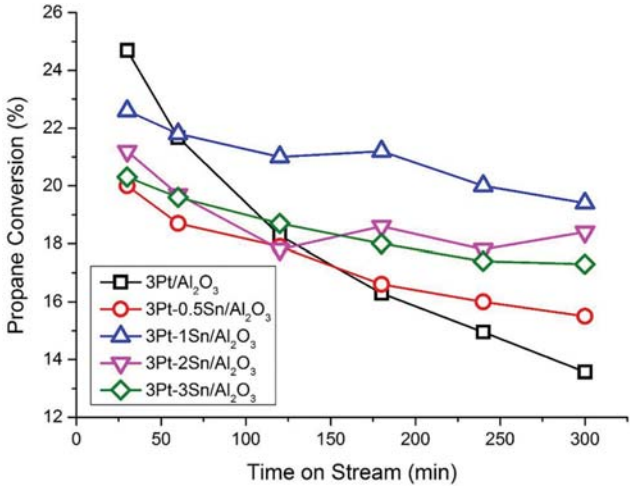

Fig. 1. Catalyst performance in propane conversion during 5 h reaction. Reaction conditions: T=600 °C, catalyst loading=0.1 g, C_3H_8 : H_2=1 : 1, total feed: 60 ml min^{-1}.

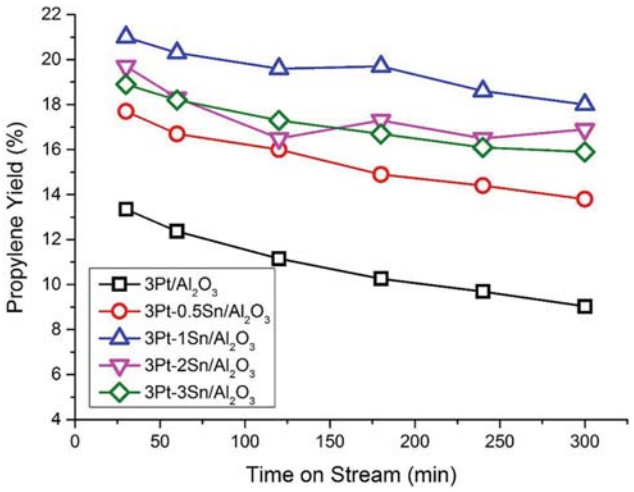

Fig. 2. Propylene yield of $3Pt/Al_2O_3$ catalysts with and without added Sn (%) during 5 h reaction.

catalyst and four other Pt-Sn/Al_2O_3 catalysts were used in this work. As mentioned earlier, four different Pt-Sn/Al_2O_3 catalysts were prepared separately and named based on the Pt and Sn contents. 3Pt-0.5Sn/Al_2O_3, 3Pt-1Sn/Al_2O_3, 3Pt-2Sn/Al_2O_3, and 3Pt-3Sn/Al_2O_3 represent 3.0 wt% Pt with different Sn content of 0.5, 1.0, 2.0, and 3.0 wt, respectively. The $3Pt/Al_2O_3$ catalyst showed the best propane conversion up to 30 min, but deactivation was noticeable after 5 h in the PDH reaction. Deactivation is mainly caused by coke generation. Once coke forms on the surface of the catalyst, the activation sites become covered, thereby terminating the reaction. In the 5 h PDH operation, the propane conversion followed the order: 3Pt-1Sn/Al_2O_3>3Pt-2Sn/Al_2O_3>3Pt-3Sn/Al_2O_3>3Pt-0.5Sn/Al_2O_3> $3Pt/Al_2O_3$ for the different catalysts. As shown in Fig. 2, the propylene selectivity followed the same order as shown in Fig. 1. The propane conversion and propylene selectivity of all the Sn-added catalysts were superior to those of the $3Pt/Al_2O_3$ catalyst.

The coke types formed after the PDH reaction with the different catalysts were evaluated by TGA (Fig. 3). The five specimens used for TGA were the spent catalysts with coke after 5 h of the PDH reaction, termed $3Pt/Al_2O_3$, 3Pt-0.5Sn/Al_2O_3, 3Pt-1Sn/Al_2O_3, 3Pt-2Sn/Al_2O_3, and 3Pt-3Sn/Al_2O_3. The numbers represent the weight percentages of each metal catalyst. In Fig. 3, the initial weight loss recorded up to 150 °C is attributed to the evaporation of moisture. The weight loss observed at 150-350 °C is assumed to be due the evaporation of organic volatiles. The relatively steep weight reduction at 350-750 °C is attributed to coke combustion. If the assignments are correct, the largest amount of coke was formed on the $3Pt/Al_2O_3$ catalyst, as expected. From comparison of the results in Fig. 3 with the data in Fig. 1 and Fig. 2, it can be concluded that the accumulated amount of coke was greatest for the $3Pt/Al_2O_3$ catalyst, and the accumulated coke negatively influenced the propane conversion and propylene selectivity. Note that the decomposition of inorganic species may occur in the temperature range of 350 to 750 °C, but this was considered negligible. For evaluation of the coke combustion kinetics, the extent of the reaction (α) shown in Eq. (2) was calculated from the determined values, as shown in Fig. 4. From the TGA data, T_0 and T_f were defined as 350 and

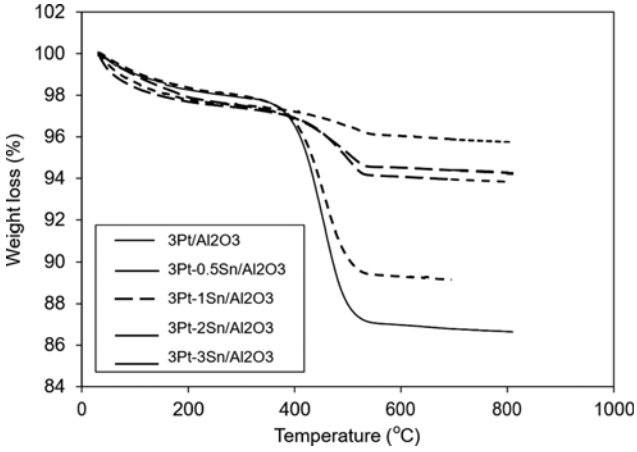

Fig. 3. TGA profile of the spent PDH catalyst, measured at the heating rate of 5 °C min^{-1}.

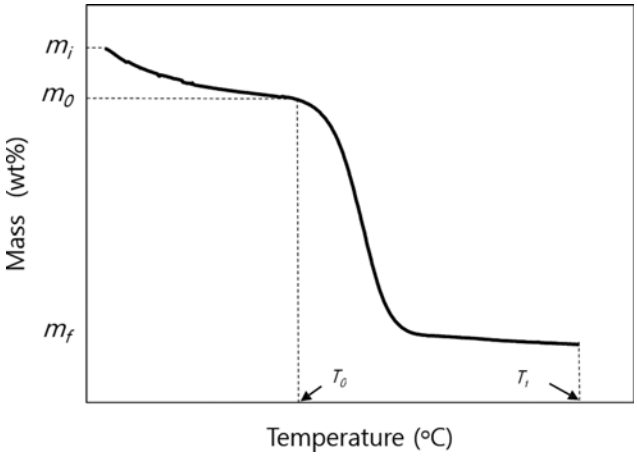

Fig. 4. Schematic diagram of determination of T_0, m_0, and m_f. T_0 and T_f were set to 350 and 750 °C, respectively.

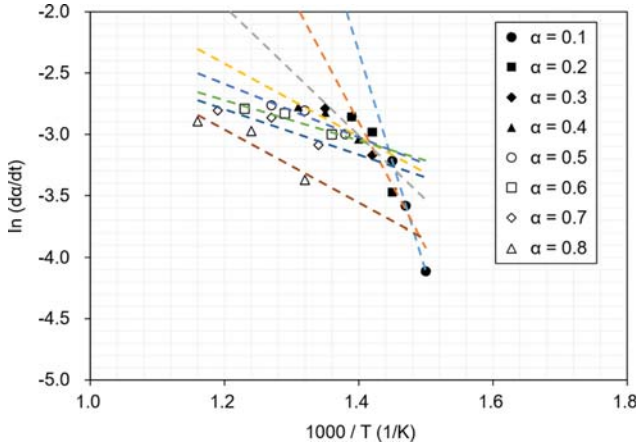

Fig. 5. Correlation between ln(dα/dt) and 1000/T for 3Pt/Al_2O_3 catalyst with respect to α.

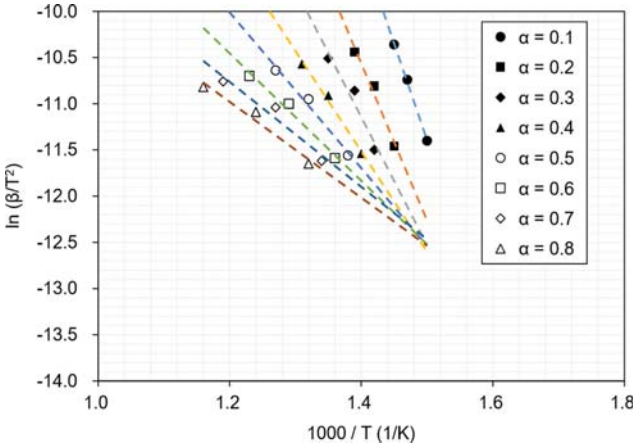

Fig. 7. Correlation between ln(β/T^2) and 1000/T for 3Pt/Al_2O_3 catalyst with respect to α.

750 °C, respectively.

As introduced earlier, three kinetic models (FR, FWO, and KAS)

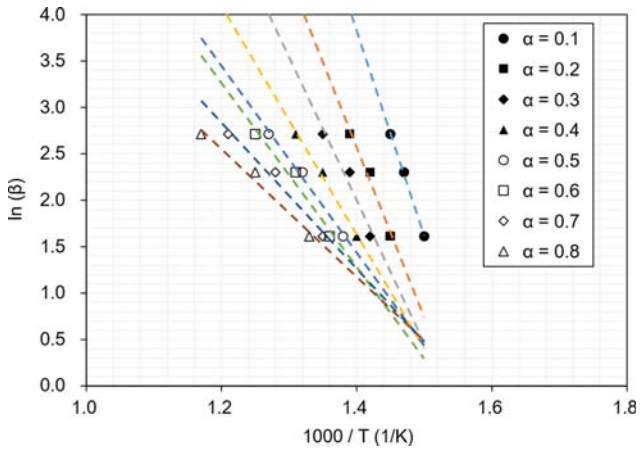

Fig. 6. Correlation between ln(β) and 1000/T for 3Pt/Al_2O_3 catalyst with respect to α.

were chosen for evaluating the activation energy. By revisiting Eq. (9) for the FR model, the activation energy can be obtained from the plot of ln(dα/dt). As shown in Fig. 5, ln(dα/dt) was plotted with respect to 1000/T for the 3Pt/Al_2O_3 catalyst. The slope obtained from Eq. (9) provides the activation energy. Integration methods such as the FWO and KAS models used herein do not provide analytical solutions for Eq. (10) but provide adequate approximate values. The activation energy could be calculated based on the approximations presented in Eq. (11) and Eq. (12). The activation energy was derived from the slopes shown in Fig. 6 and Fig. 7. Both graphs correspond to the 3Pt/Al_2O_3 catalyst. There have been studies exploring various activation energies with respect to conversions. Major studies show varying activation energies as a function of conversion for oil shale pyrolysis (retorting) and biomass pyrolysis. To our knowledge, the varying activation energies are related to the mixtures of products. If there is a single product or a dominant product with minimal side products, the single activation energy may work efficiently. However, the products from thermal decomposition may have diverse products with different properties. In this case of PDH, we claim that there are diverse products generated from thermal decomposition. It is true that there are different compounds in cokes, such as aliphatics, aromatics, and graphites, and we thought that these three major compounds may have wider ranges of molecular weight. This is the approach that

Table 2. Activation energy (E_a) and pre-exponential factor (A) from Friedman (FR), Kissinger-Akahira-Sunose (KAS), Flynn-Wall-Ozawa (FWO), and Kissinger methods

	3Pt/Al_2O_3								
Conversion (α)	FR			KAS			FWO		
	E_a (kJ/mol)	A (min^{-1})	R^2	E_a (kJ/mol)	A (min^{-1})	R^2	E_a (kJ/mol)	A (min^{-1})	R^2
0.1	171.60	4.8E+11	0.9984	199.80	2.1E+05	0.9921	200.63	1.5E+14	0.9930
0.2	94.41	5.7E+05	0.9120	156.31	8.8E+01	0.9840	159.70	6.5E+10	0.9862
0.3	43.50	1.1E+02	0.8664	113.22	7.0E−02	0.9668	119.05	5.3E+07	0.9729
0.4	23.31	4.2E+00	0.8649	85.56	9.1E−04	0.9648	93.02	7.0E+05	0.9733
0.5	17.23	1.8E+00	0.8807	67.88	6.6E−05	0.9673	76.48	5.1E+04	0.9771
0.6	13.26	1.1E+00	0.8866	56.39	1.3E−05	0.9688	65.83	1.0E+04	0.9798
0.7	15.61	1.9E+00	0.9009	47.68	4.4E−06	0.9669	57.81	3.4E+03	0.9804
0.8	24.27	8.5E+00	0.8691	42.52	2.4E−06	0.9598	53.21	2.0E+03	0.9777

Table 2. Continued

3Pt-0.5Sn/Al_2O_3									
Conversion (α)	FR			KAS			FWO		
	E_a (kJ/mol)	A (min^{-1})	R^2	E_a (kJ/mol)	A (min^{-1})	R^2	E_a (kJ/mol)	A (min^{-1})	R^2
0.1	181.71	3.2E+12	0.9872	226.60	2.9E+07	0.9913	226.02	2.0E+16	0.9921
0.2	124.50	9.9E+07	0.9619	174.73	2.1E+03	1.0000	177.15	1.5E+12	1.0000
0.3	64.80	3.7E+03	0.8705	132.44	1.6E+00	0.9914	137.27	1.2E+09	0.9929
0.4	33.59	2.3E+01	0.7719	96.04	4.7E−03	0.9777	102.95	3.6E+06	0.9827
0.5	19.90	2.9E+00	0.6728	76.82	2.5E−04	0.9620	84.95	2.0E+05	0.9721
0.6	12.25	9.8E−01	0.4259	62.34	3.2E−05	0.9572	71.45	2.5E+04	0.9709
0.7	16.78	2.3E+00	0.6060	52.53	8.6E−06	0.9460	62.40	6.9E+03	0.9658
0.8	22.09	5.8E+00	0.6575	45.29	3.5E−06	0.9399	55.84	2.9E+03	0.9648
3Pt-1Sn/Al_2O_3									
Conversion (α)	FR			KAS			FWO		
	E_a (kJ/mol)	A (min^{-1})	R^2	E_a (kJ/mol)	A (min^{-1})	R^2	E_a (kJ/mol)	A (min^{-1})	R^2
0.1	239.69	1.3E+16	0.9134	370.73	4.4E+16	0.9393	363.74	3.5E+25	0.9429
0.2	175.42	1.9E+11	0.9949	235.38	6.8E+06	0.9778	235.38	5.6E+15	0.9799
0.3	149.14	2.0E+09	0.9933	194.96	8.6E+03	0.9942	197.19	7.3E+12	0.9949
0.4	138.26	3.1E+08	0.9902	178.57	5.6E+02	0.9997	181.82	4.9E+11	0.9997
0.5	127.28	5.1E+07	0.9898	153.85	1.2E+01	0.9997	158.52	1.0E+10	0.9997
0.6	132.61	1.2E+08	0.9973	153.18	9.6E+00	0.9990	158.06	8.8E+09	0.9992
0.7	141.28	4.6E+08	0.9992	148.44	4.5E+00	0.9995	153.73	4.3E+09	0.9996
0.8	162.11	1.0E+10	0.9992	147.69	4.0E+00	0.9989	153.18	3.8E+09	0.9990
3Pt-2Sn/Al_2O_3									
Conversion (α)	FR			KAS			FWO		
	E_a (kJ/mol)	A (min^{-1})	R^2	E_a (kJ/mol)	A (min^{-1})	R^2	E_a (kJ/mol)	A (min^{-1})	R^2
0.1	622.78	3.0E+44	0.9272	854.13	1.0E+52	0.9654	823.14	8.3E+60	0.9663
0.2	351.98	1.3E+24	0.9669	440.95	3.2E+21	0.9641	430.64	2.6E+30	0.9659
0.3	248.25	2.4E+16	0.9916	312.83	1.5E+12	0.9852	309.09	1.3E+21	0.9863
0.4	205.88	1.6E+13	0.9947	259.31	1.9E+08	0.9953	258.46	1.6E+17	0.9957
0.5	199.85	4.3E+12	0.9986	243.63	1.1E+07	0.9976	243.77	9.7E+15	0.9978
0.6	168.75	2.9E+10	0.9960	202.02	1.5E+04	0.9987	204.43	1.4E+13	0.9988
0.7	177.02	9.5E+10	0.9978	191.19	2.4E+03	0.9957	194.33	2.3E+12	0.9962
0.8	201.17	3.0E+12	0.9997	191.48	2.1E+03	0.9985	194.79	2.1E+12	0.9987
3Pt-3Sn/Al_2O_3									
Conversion (α)	FR			KAS			FWO		
	E_a (kJ/mol)	A (min^{-1})	R^2	E_a (kJ/mol)	A (min^{-1})	R^2	E_a (kJ/mol)	A (min^{-1})	R^2
0.3	714.09	2.4E+48	0.8714	865.85	6.4E+49	0.7799	834.96	5.7E+58	0.7848
0.4	469.15	5.2E+30	0.9892	584.65	4.5E+29	0.9981	567.93	4.2E+38	0.9982
0.5	434.33	6.2E+27	0.9997	505.87	5.3E+23	0.9908	493.33	5.2E+32	0.9913
0.6	317.12	5.3E+19	0.9679	350.15	1.6E+13	0.9951	345.54	1.6E+22	0.9954
0.7	496.96	6.4E+30	0.9841	370.90	1.4E+14	0.9632	365.53	1.4E+23	0.9656

we tried to fractioned activation energies of cokes decomposing at different temperatures. In Fig. 5, the y-axis represents ln(β) and the x-axis is 1000/T. The activation energies for the 3Pt-0.5Sn/Al_2O_3, 3Pt-1Sn/Al_2O_3, 3Pt-2Sn/Al_2O_3, and 3Pt-3Sn/Al_2O_3 catalysts were calculated and are summarized in Table 2. Notably, the activation energy increased as the Sn addition increased. For the 3Pt/Al_2O_3 and 3Pt-0.5Sn/Al_2O_3 catalysts, the KAS model had the highest R^2 values, indicating that this model provided the best fit for the data. However, for the other three catalysts (3Pt-1Sn/Al_2O_3, 3Pt-2Sn/Al_2O_3, and 3Pt-3Sn/Al_2O_3), the data fit of the models did not differ significantly (Table 2). The pre-exponential factor, A, was determined based on the assumption of a first-order reaction (F1, refer to Table 1).

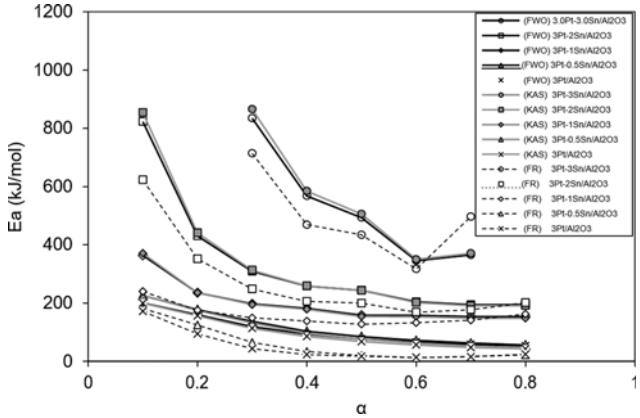

Fig. 8. Activation energy with respect to α, calculated by using FWO, KAS, and FR models.

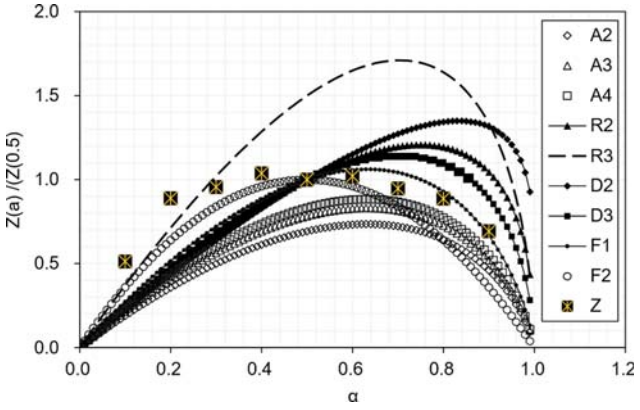

Fig. 9. Criado master-plot represented by $Z(\alpha)/Z(0.5)$ for $3Pt/Al_2O_3$ catalyst.

The calculated activation energy values are plotted with respect to α in Fig. 8. Three methods and five individual catalysts were evaluated. Overall, the $3Pt/Al_2O_3$ catalyst had the lowest energy. The activation energy increased with increasing Sn addition. Comparison of the three models shows that the FWO model and KAS model provided similar fits. As a differential method, the FR model deviated from the FWO and KAS models for all five catalysts, providing the lowest values. Based on the variance of the β values, $z(\alpha)$ fitting was not satisfied in this work. Complicated steps during coke combustion may be possible. However, herein, the activation energy was evaluated using non-isothermal conversion methods. As mentioned, the activation energy was notably higher when more Sn was added and the activation energy was highest with the 3Pt-3Sn/Al_2O_3 catalyst (Table 2).

When we interpret the combustion phenomena, several issues arise as listed below:

- The location of the coke species that affect the combustion kinetics
- Qualitatively different components may result in different activation energy
- The combustion rate may be dependent upon α.

First, the coke species may be localized either near the Pt metal or near SnO_2. If the coke is localized near the Pt sites, combustion would be accelerated under oxygen atmosphere [1-3]. As shown in Fig. 8, the $3Pt/Al_2O_3$ catalyst had the lowest activation energy. Second, it was reported that different constituents of coke were possible, such as aliphatic, aromatic, and pre-graphitic [8]. With increasing Sn addition in the range of 0.5-3.0 wt%, less coke was generated in the 5 h PDH reaction and the activation energy for coke combustion became higher. Third, there is an evidence that the reaction rate may follow more than one model, such as a combination of first-order and second-order kinetics. Note that a simplified interpretation of the combustion kinetics may be enough for analysis, even with one rate model. In this work, first-order kinetics was adopted for further calculation of the pre-exponential values accompanying the activation energy calculation. Nevertheless, a detailed understanding of all the issues highlighted here requires further experimental studies.

In Fig. 9, the first-order (F1, refer to Table 1) reaction was selected for application to Eq. (11) and Eq. (12). In the rage of α<0.5, the second-order (F2, refer to Table 1) model provided the best fit. However, in the range of α>0.5, the first-order (F1) model provided a better fit to the experimental data. This analysis is known as the Criado master-plot [29,30]. This analysis is explained elsewhere [18,21]. One objective of the Criado master-plot method is to determine $f(\alpha)$ and $g(\alpha)$. $G(\alpha)$ is the integral form of $f(\alpha)$, as mentioned earlier. Herein, the experimental values were analyzed by the Criado method. Interestingly, two candidate functions (F1 and F2) fit the experimental data. This may be the reason why two regimes were observed in the TGA plots. In the relatively low temperature region below 450 °C, pseudo-pyrolysis conditions might be possible. However, oxygen combustion may proceed in a different manner in the higher temperature range of 450 °C or higher. Further studies would be required to classify the effect of the pyrolysis kinetics and oxidative combustion kinetics.

CONCLUSION

Pt/Al_2O_3 catalyst as a reference and four different $Pt\text{-}Sn/Al_2O_3$ catalysts were prepared for the PDH reaction with variation of the Pt/Sn ratio from 3.0 : 0.5 to 3.0 : 3.0 by weight. The addition of Sn metal as a co-catalyst enhanced the propane conversion and propylene selectivity. During the PDH reaction, side reactions on the catalyst surface resulted in coke generation and deposition on the surface of the catalyst. Because coke weakens the catalytic activity, coke burning is inevitable. In this study, the kinetics of coke combustion were evaluated to determine the activation energy, as well as the activation energy with Sn addition to the Pt/Al_2O_3 catalyst. Thermal gravimetric analysis was employed to determine the amount of coke deposited and to calculate the kinetic parameters for coke combustion. Three non-isothermal models (Friedman, Flynn-Wall-Ozawa (FWO), and Kissinger-Akahira-Sunose (KAS)) were used to determine the activation energy and find the best model to fit the experimental data. In the case of $3Pt/Al_2O_3$ and $3Pt\text{-}0.5Sn/Al_2O_3$, the FWO model provided the best fit to the data. The three models provided similar fits in the case of $3Pt\text{-}1Sn/Al_2O_3$, $3Pt\text{-}2Sn/Al_2O_3$, and $3Pt\text{-}3Sn/Al_2O_3$. The results show that the activation energy was higher when the addition of Sn to the Pt/Al_2O_3 cata-

lyst was increased. It is suspected that the localization of coke near the Pt site may be advantageous for accelerating the combustion reaction. Increasing the addition of Sn to the Pt/Al_2O_3 catalyst may generate coke with much higher molecular weights. When the experimental data were plotted using the Criado master-plot method, two different reaction orders were observed. The second-order reaction was operative in the range of $\alpha<0.5$, and the first-order reaction dominated at $\alpha>0.5$. These mixed results were attributed to differences in the reaction during TGA analysis. Pseudo-pyrolysis and oxidative combustion might affect the TGA analysis to different extents. Further studies would be required to confirm a shift in the reaction from pyrolysis to combustion.

ACKNOWLEDGEMENTS

This work was financed by the industry core-technology project termed "Development of High Yield Propylene Production Process Technology" of the Ministry of Trade, Industry, and Energy (project No.: 100052754; Korea Evaluation Institute of Industrial Technology), and by the Basic Science Research Program through the National Research Foundation of Korea (NRF) funded by the Ministry of Education (2017R1D1A1B03034244).

REFERENCES

1. J. J. H. B. Sattler, J. Ruiz-Martinez, E. Santillan-Jimenez and B. M. Weckhuysen, *Chem. Rev.*, **114**, 10613 (2014).
2. Z. Nawaz, *Rev. Chem. Eng.*, **31**, 413 (2015).
3. M. M. Bhasin, J. H. McCain, B. V. Vora, T. Imai and P. R. Pujadó, *Appl. Catal. A Gen.*, **221**, 397 (2001).
4. S. M. Stagg, C. A. Querini, W. E. Alvarez and D. E. Resasco, *J. Catal.*, **168**, 75 (1997).
5. B. V. Vora, *Top. Catal.*, **55**, 1297 (2012).
6. J. J. H. B. Sattler, I. D. Gonzalez-Jimenez, L. Luo, B. A. Stears, A. Malek, D. G. Barton, B. A. Kilos, M. P. Kaminsky, T. Verhoeven, E. J. Koers, M. Baldus and B. M. Weckhuysen, *Angew. Chem. Int. Ed.*, **53**, 9251 (2014).
7. J.-W. Jung, W.-I. Kim, J.-R. Kim, K. Oh and H. L. Koh, *Catalysts*, **9**, 446 (2019).
8. H.-Z. Wang, L.-L. Sun, Z.-J. Sui, Y.-A. Zhu, G.-H. Ye, D. Chen, X.-G. Zhou and W.-K. Yuan, *Ind. Eng. Chem. Res.*, **57**, 8647 (2018).
9. A. Ochor, A. Ibarra, J. Bilbao, J. M. Arandes and P. Castano, *Chem. Eng. Sci.*, **171**, 459 (2017).
10. P. B. Weisz and R. B. Goodwin, *J. Catal.*, **6**, 227 (1966).
11. P. B. Weisz, *J. Catal.*, **6**, 425 (1966).
12. P. K. Doolin, J. F. Hoffman and M. M. Mitchell Jr., *Appl. Catal.*, **71**, 233 (1991).
13. I. V. Babich, K. Seshan and L. Lefferts, *Appl. Catal. B Environ.*, **59**, 205 (2005).
14. A. N. Zagoruiko, A. S. Belyi, M. D. Smolikov and A. S. Noskov, *Catal. Today*, **220**, 168 (2014).
15. M. Mehraban and B. H. Shahraki, *Fuel Process. Technol.*, **188**, 172 (2019).
16. S. Luo, S. He, X. Li, J. Li, W. Bi and C. Sun, *Fuel Process. Technol.*, **129**, 156 (2015).
17. P. Tiwari and M. Deo, *AIChE J.*, **58**, 505 (2012).
18. P. Das and P. Tiwari, *Thermochim. Acta*, **654**, 191 (2017).
19. T. U. Han, Y.-M. Kim, A. Watanabe, N. Teramae, Y.-K. Park and S. Kim, *Korean J. Chem. Eng.*, **34**, 1214 (2017).
20. J. W. Kim, S.-H. Lee, S.-S. Kim, S. H. Park, J.-K. Jeon and Y.-K. Park, *Korean J. Chem. Eng.*, **28**, 1867 (2011).
21. P. Bartocci, R. Tschentscher, R. E. Stensrød, M. Barbanera and F. Frantozzi, *Molecules*, **24**, 1657 (2019).
22. H. L. Friedman, *J. Polym. Sci. C*, **6**, 183 (1964).
23. H. Kissinger, *J. Res. Natl. Bur. Stand.*, **57**, 217 (1956).
24. T. Akahira and T. Sunose, *Res. Rep. Chiba. Inst. Technol.* (*Sci. Technol.*), **16**, 22 (1971).
25. T. Ozawa, *Bull. Chem. Soc. Japan*, **38**, 1881 (1965).
26. J. H. Flynn and L. A. Wall, *Polym. Lett.*, **4**, 323 (1966).
27. C. D. Doyle, *J. Appl. Polym. Sci.*, **6**, 639 (1961).
28. J. M. Criado, *Thermochim. Acta*, **24**, 186 (1978).
29. I. A. Pérez-Maqueda, J. M. Criado, F. J. Gotor and J. Málek, *J. Phys. Chem. A*, **106**, 2862 (2002).